Prepared for the National Institutes of Health
National Institute of Neurological Disorders and Stroke
Division of Stroke, Trauma and Neurodegenerative Disorders
Neural Prosthesis Program
Bethesda, MD 20892

Microstimulation of the Lumbosacral Spinal Cord: Mapping

NIH-NINDS-NO1-NS-8-2300

Quarterly Progress Report #3

Period Covered: 1 April, 1999 - 30 June, 1999

Principal Investigator: Warren M. Grill, Ph.D.

Co-Investigators: Musa A. Haxiu, M.D., Ph.D.
Michel A. Lemay, Ph.D.

Department of Biomedical Engineering
Case Western Reserve University
Cleveland, OH 44106-4912

ABSTRACT

The objectives of this research are to determine the anatomical locations of spinal neurons involved in control of the genitourinary and hindlimb motor systems, and to determine the physiological responses evoked in the genitourinary and hindlimb motor systems by intraspinal microstimulation. During this quarter we made progress toward both of these objectives. We continued a series of experiments to characterize the hindlimb motor responses evoked by microstimulation of the lumbar spinal cord. We measured the endpoint forces evoked by intraspinal microstimulation of the lumbar spinal cord in decerebrate cats and compared these response to those obtained in anesthetized α-chloralose, preparations. We also continued work on an electrical technique to localize neurons in the spinal cord using recordings of electrical potential on the surface of the spinal cord. During this quarter we developed, implemented, and verified analytical solutions for the potentials generated in two cylindrical volume conductor models of the spinal cord.

INTRODUCTION

Electrical stimulation of the nervous system is a means to restore function to individuals with neurological disorders. The objective of this project is to investigate the feasibility of neural prosthetics based on microstimulation of the spinal cord with penetrating electrodes. Specifically, chemical and viral retrograde tracers, immediate early gene expression, and immunocytochemistry are used to determine the locations and neurochemical identity of neurons in the spinal cord that control genitourinary and motor functions in the male cat. Microstimulation with penetrating activated iridium microelectrodes is used to determine the physiological effects in the genitourinary and motor systems of activation of different neural populations. The results of this project will provide data important to understanding neural control of genitourinary and motor functions, answer fundamental questions about microstimulation of the spinal cord, and lead to development of a new generation of neural prosthetics for individuals with neurological impairments.

PROGRESS IN THIS QUARTER

During the second quarter of this contract we continued a series of experiments to measure the endpoint force produced at the hindlimb by microstimulation of the lumbar spinal cord. We also continued work on an electrical technique to localize neuronal populations within the spinal cord. Below each of our accomplishments is summarized.

Hindlimb Motor Responses Evoked by Intraspinal Microstimulation

We are conducting a series of experiments to characterize the hindlimb motor responses evoked by microstimulation. In these experiments rather than recording single joint responses, we are recording the net force at the endpoint of the hindlimb. During the period covered by this report, we studied the spinal mapping of motor responses evoked by intraspinal microstimulation of the lumbar enlargement of the spinal cord in two animals. In contrast to our previous experiments, which were conducted in animals anesthetized with α-chloralose, a new unanesthetized, decerebrate preparation was used.

METHODS

The endpoint forces evoked at the paw by microstimulation of the lumbar spinal cord were recorded in unanesthetized decerebrate cats. All animal care and experimental procedures were according to NIH guidelines and were approved by the Institutional Animal Care and Use Committee of Case Western Reserve University.

Experimental Preparation

Animals were anesthetized with ketamine HCl (Ketaset, 15-30 mg/kg, IM), intubated, and anesthesia was maintained with gaseous halothane (1-2 %) in oxygen. A laminectomy was made to expose the lumbosacral spinal cord, and the contralateral (left) hindlimb was denervated by transecting the femoral, obturator, and sciatic nerves. Denervation was done to prevent mechanical coupling of crossed responses in the left limb to the force sensor to which the right limb was attached. The animal was mounted in a frame with pins at the hips, the head in a headholder, and vertebral clamps at L3 and S1. The femur was fixed with a steel pin, and the paw was attached to a gimbal mounted on a 3-axis force/moment transducer (Nano-17, ATI Inc., Garner, NC). The force transducer was mounted on a cartesian manipulator that allowed positioning of the force sensor throughout the workspace of the lower leg and paw, while the gimbal permits the rotation of the ankle when the limb is moved. Fine bifilar wire electrodes were inserted into four hindlimb muscles (knee flexor, knee extensor, ankle flexor, and extensor) to record the electromyographic (EMG) activity. Body temperature was maintained between 37° and 39° C with a thermostatically controlled heat lamp. 0.9% saline with 8.4 mg/cc sodium bicarbonate and 5% dextrose added was administered IV (~20 cc/hr), and artificial respiration was used to maintain the end tidal CO2 at 3-4%. The carotid arteries were ligated and the left carotid was catheterized to monitor arterial blood pressure. Dexamethasone (2 mg/kg) was administered at the completion of the laminectomy and every 6 hours thereafter for the duration of the experiment. Following surgical preparation, a midcollicular decerebration was conducted and halothane anesthesia discontinued. At least one hour elapsed between the end of anesthesia and the onset of data collection.

Stimulation

The dura was opened, the levels were identified by root exit, the spinal cord was covered with warm mineral oil, and microstimulation commenced. Vertical, dorsal-to-ventral penetrations were made to position electrodes at locations identified in our previous high-resolution mapping studies to evoke hindlimb motor responses. Activated iridium wire microelectrodes (50 μm diameter) with an exposed electrochemically determined surface area of ~225 μm^2, a 1-3 μm tip, and insulated with Epoxylite were used (IS300, Huntington Medical Research Institutes, Pasadena, CA). Stimuli were

charge balanced biphasic pulses with a cathodic phase amplitude of 10-100 μA and duration of 100 μs applied at 40 Hz for 0.5 s. The amplitude of the anodic phase was limited to 100 μA and the duration was set automatically by the stimulator to balance the charge in the primary phase.

Data Collection and Analysis

At selected depths along each penetration the limb was moved on a 3 cm grid of nine to twelve points from a mid-stance position while the stimulation parameters and electrode position were kept constant (see Fig. 2.1, QPR #2). The forces measured at those nine to twelve locations were used to calculate the forces acting on the limb's endpoint throughout the workspace [Giszter et al., 1993]. The workspace was divided into triangles, and the forces within a triangle were estimated by a linear interpolation based on the three vectors measured on the vertices (see QPR #2). Note that although we measured forces and moments along three orthogonal axes (x, y and z) our analysis was limited to the sagittal plane. Furthermore, the forces were divided into a passive component (force measured before the onset of activation), and an active component (total forces measured minus the passive portion). Total, active and passive force fields were reconstructed. The forces due to gravity were calculated using simple mechanics and subtracted out. The ankle and knee moments due to gravity were calculated from the cat's weight and segment lengths obtained from post-mortem x-rays [Hoy and Zernicke, 1985].

The torques acting at the knee and ankle joints are calculated from the force measurements and are given by $\mathbf{T}=\mathbf{J}^{\mathrm{T}}\mathbf{F}$, where $\mathbf{T}$ is the torque vector (knee, ankle), $\mathbf{F}$ is the force vector (Fx, Fy), and $\mathbf{J}^{\mathrm{T}}$ is the transpose of the limb's Jacobian. Calculating the Jacobian requires the link lengths (obtained via post-mortem X-rays of the animal), and joint angles (calculated using link length measurements, and the position of the knee joint relative to the force sensor).

The electromyographic (EMG) activity of four hindlimb muscles was measured simultaneously with the evoked forces. EMG was measured from *biceps femoris*, *vastus medialis*, *tibialis anterior*, and *medial gastrocnemius*, and electrode locations were verified via post-mortem dissection. The raw EMG signals were amplified, filtered (10-1000Hz), and sampled at 2500Hz.

RESULTS

The results in the decerebrate preparation were, for the most part, similar to the results in the anesthetized (α-chloralose) preparation. Responses to electrical stimulation and reflexes were heightened, such that forces and EMGs tended to be higher for the same stimulation level. We characterized a total of nine fields over three ipsilateral penetrations in two animals. The majority of the active fields (5 of 9) were flexion withdrawal responses, as observed in the anesthetized preparation (See fig. 2.3A, QPR #2). The remaining fields were either caudal extensor (three), or atypical extensor (one) that had not been previously observed.

The atypical extensor field is shown in figure 3.1. The position of each vector is plotted at the position of the limb endpoint where it was measured, its length is proportional to the force magnitude, and its direction indicates the direction of the endpoint force. In contrast to caudal extensor fields (see fig. 2.3C, QPR #2), the direction

of the endpoint extension force was not directed strictly in the caudal or rostral direction, but rather varied with the position of the limb endpoint.

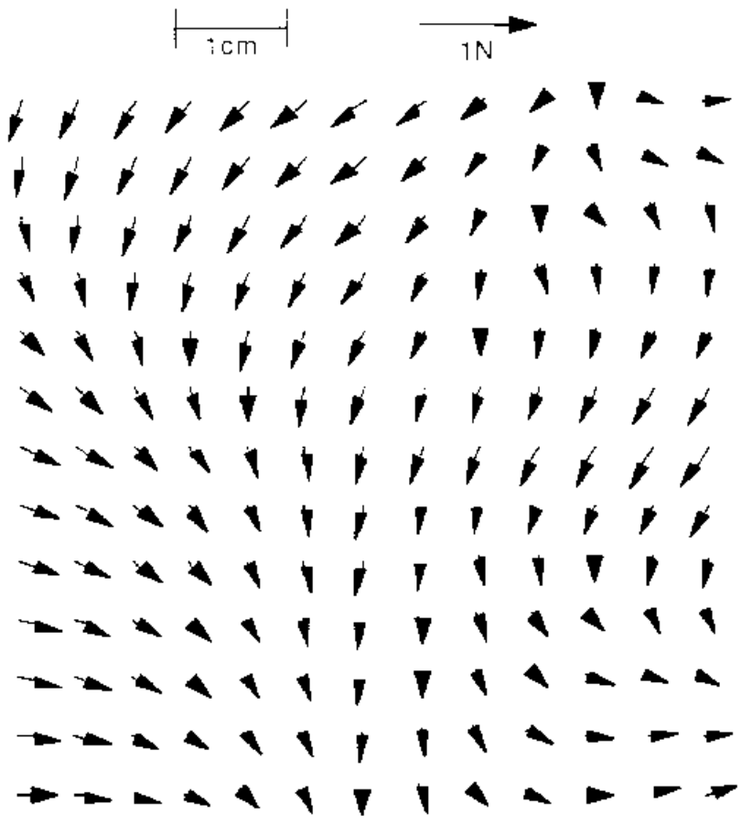

Figure 3.1 Atypical force pattern observed in one of the penetration. Depth of observation was 3800μm at the L6/L7 border near the dorsal root entry zone. (SFF05).

This field also displayed another property that had not been observed in the anesthetized animals. The direction of the force vector elicited varied over the time course of the response for a number of limb positions. An example of the temporal evolution of the endpoint force is shown in fig. 3.2. The length and magnitude of the vectors correspond to the endpoint force vectors, and the force vectors are plotted at discrete time points before, during, and after the stimulus. This behavior was not observed during any of the other fields, although an off-response was elicited on some trials. The off response consisted of a large force response that occurred after the end of stimulation train. These responses were not observed in the anesthetized (α-chloralose) preparation, presumably due to the suppression of the reflex circuitry caused by the anesthetic.

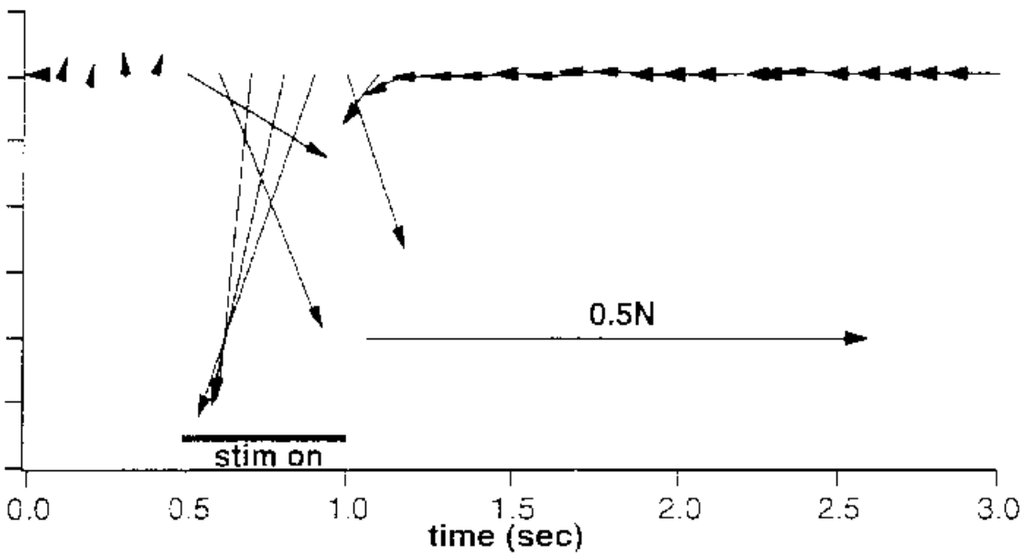

Figure 3.2. Time course of the force vector at one position for the atypical extensor displayed in Fig. 3. Notice how the vector rotates during the stimulation period (indicated by the solid bar between 0.5 and 1.0 sec). This behavior was only observed for this particular field.

As in our previous experiments (see fig. 3.2, QPR #2), the passive force fields (i.e., endpoint force vectors generated by the passive properties of the limb in the absence of any stimulation) were very similar across animals (fig. 3.3). Both fields showed increasing extension forces as the leg was flexed, and decreasing extension forces, with a transition to flexion forces, as the leg was extended. In the rostral-caudal direction, the passive forces in SFF05 tended to restore the limb towards a neutral position, while the restoring forces in SFF06 were oriented caudally, presumably because the workspace grid was centered over a more rostral position. In those two examples, the leg was sufficiently extended to show the expected reversal from extension forces to flexion forces as the limb was further extended.

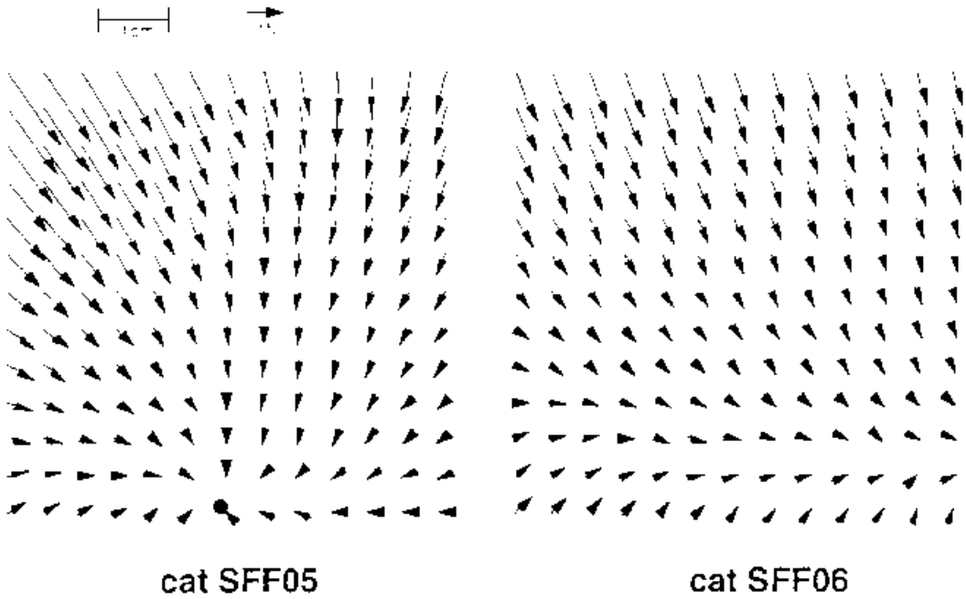

Figure 3.3. Passive force field (without gravity) for both animals (SFF05 and SFF06). The animal placement was ideal for SFF05, and the passive forces measured show the expected point of convergence (forces going to zero) within the workspace used for measurement. The animal was probably mounted too forward in SFF06, and the leg should have been stretched further back to show the forward pointing restoring forces. Both fields indicate that the animal's limb is now sufficiently extended to demonstrate flexion restoring forces.

CONCLUSIONS

Our measurements of endpoint forces in decerebrate, spinal-intact cats indicate that stimulation in the dorsal and intermediate aspects of the spinal cord generated organized, convergent force patterns, similar to those found in the anesthetized preparation. Further, the results demonstrate that much larger forces and a wider variety of response types were elicited in the unanesthetized preparation.

These results suggest that microstimulation of the mammalian spinal cord can be used to activate groups of muscles to produce organized force patterns at the limb's endpoint. This finding may find application in neural prosthetic control of multi-joint movement in persons with spinal cord injury.

Source Localization for Electrical Mapping of Spinal Neurons

The objective of this project is to develop an intraoperative mapping technique to identify the location of the neurons targeted for stimulation. We have previously developed techniques for spinal cord mapping in animal models using electrical stimulation as well as immediate early gene expression [Grill et al., 1998]. However, less invasive methods are required for in vivo mapping.

Therefore, we are undertaking to develop a solution of the inverse problem: given the potentials on the surface of the spinal cord, reconstruct the location of the source that produced those potentials [Oostendorp and Van Oosterom, 1989]. During this quarter we extended our previous work and implemented and validated two cylindrical volume conductor models of the spinal cord: a single cylinder of uniform conductivity, and a pair of concentric cylinders of differing conductivity.

METHODS

Our original intent was to use a previously developed analytical solution [Cornelis and Nyssen, 1985] as the basis of the model, however, this was not possible because the solution is valid only for a zero external conductivity (σ_e=0), which is not representative of the cerebrospinal fluid. Thus, we turned to a second solution in the literature [Meier et al., 1998], but we were unable to verify their solution (i.e., the boundary conditions were not satisfied by the published solution). We therefore elected to derive our own analytical solutions.

We have derived solutions for the potentials generated by point current sources in two different volume conductor models (figs. 3.4, 3.5). In both cases the solution involves a summation of Bessel functions, and the solutions were implemented using a Fourier solution method [Altman and Plonsey, 1988], see QPR #2, in MATLAB.

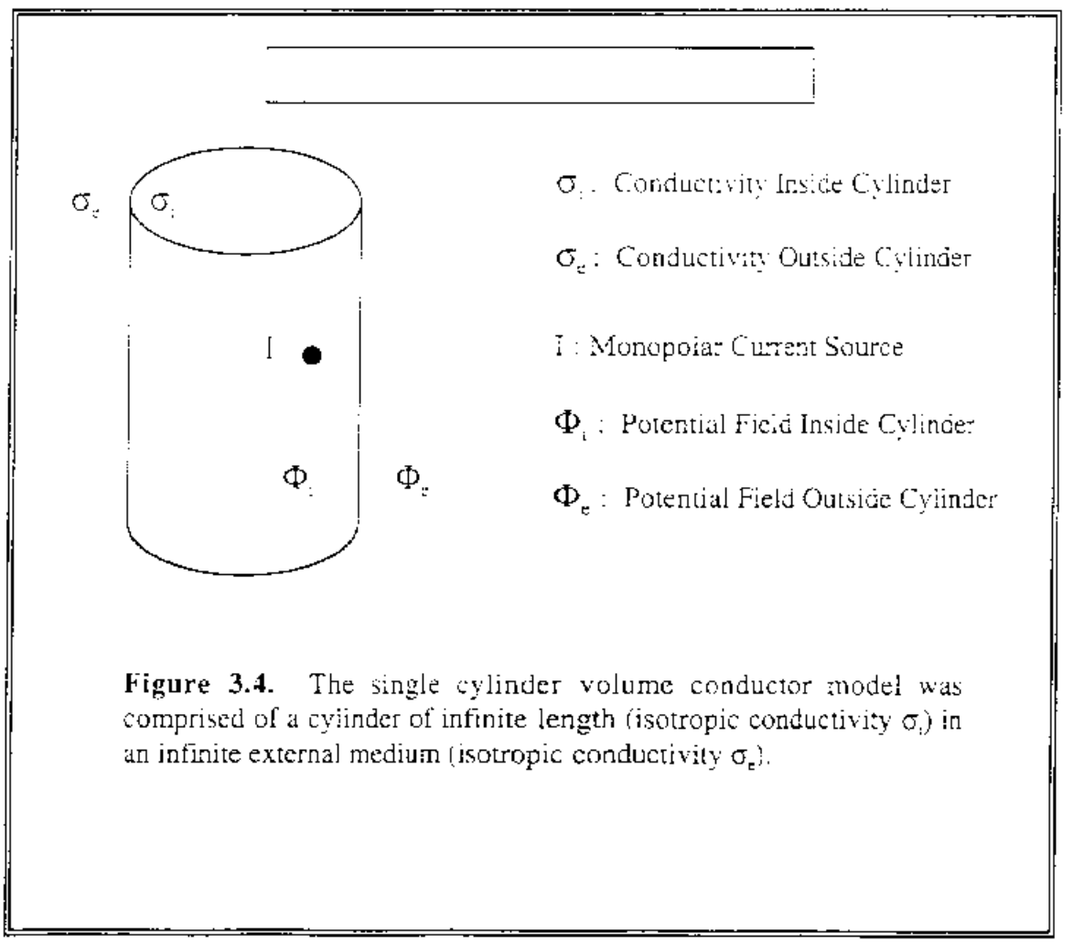

Figure 3.4. The single cylinder volume conductor model was comprised of a cylinder of infinite length (isotropic conductivity σ_i) in an infinite external medium (isotropic conductivity σ_e).

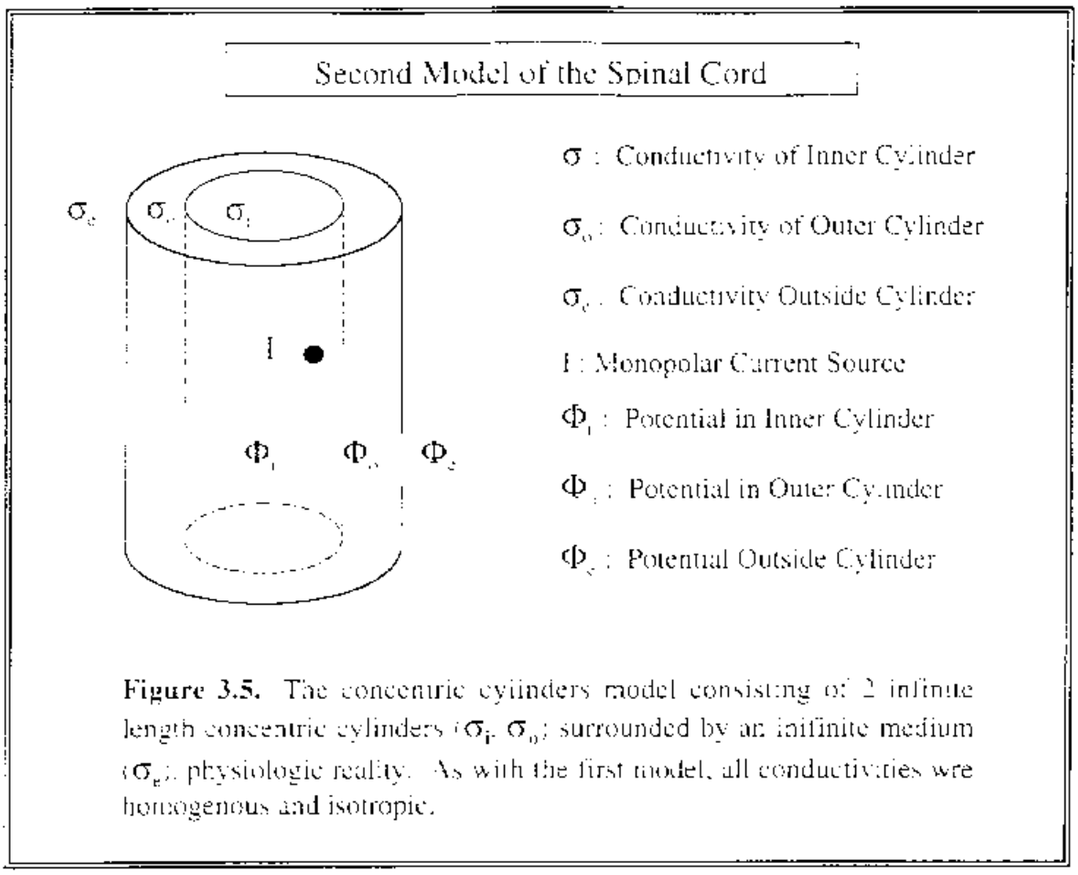

Figure 3.5. The concentric cylinders model consisting of 2 infinite length concentric cylinders (σ_i, σ_o) surrounded by an infinite medium (σ_e), physiologic reality. As with the first model, all conductivities are homogenous and isotropic.

RESULTS

We have successfully developed and implemented two cylindrical volume conductor models of the spinal cord. The first model (fig. 3.4) consists of an infinite length cylinder with isotropic conductivity, representative of the spinal cord, surrounded by an infinite homogeneous isotropic medium of different conductivity. The second model (fig. 3.5) consists of a pair of infinite length concentric cylinders of differing conductivity, representative of the gray and white matter of the spinal cord, surrounded by an infinite homogeneous isotropic medium of different conductivity.

The solutions to Poisson's equation were obtained, and subsequent verification of the boundary conditions was calculated using Mathematica (Wolfram Research). These calculations verified that all boundary conditions were satisfied. The models were implemented in Matlab (The Mathworks, Inc.), and the following tests were conducted to verify the solutions and implementations:

1. First Model converges to Point Source Model for $\sigma_i = \sigma_e$.
2. Second Model converges to First Model for $\sigma_i = \sigma_o$ (2nd model conductivities) where cylinder radii and First Model conductivities are appropriately adjusted.
3. Second Model converges to First Model for $\sigma_o = \sigma_e$ (2nd model conductivities) where cylinder radii and First Model conductivities are appropriately adjusted.
4. Second Model converges to Point Source Model for $\sigma_i = \sigma_o = \sigma_e$.

In all 4 cases, the results of these tests demonstrated that our solutions were correct and the potentials of the different models converged to an error of less than 1×10^{-6}, an error attributable to round-off.

The analytical solutions that are the bases of the models require that an infinite number of terms be summed to provide an exact solution. This is clearly not possible; however, the lower order terms contribute significantly more to the solution than do higher order terms. We conducted an analysis to determine the contribution of higher order terms to the solution so that a suitable number of frequency domain samples can be selected for the solution. The second concentric cylinders model was used for this evaluation.

The second model simulation was run 24 times; each time 512 terms were added in z frequency space for every theta in frequency space. The graph in figure 3.6 shows the potential as a function of the z-axis position for increasing numbers of samples in the z frequency space. As additional, higher-order terms were added to the solution, it converged, demonstrating that the higher order terms contributed little to the solution. This contributions is quantified (as percentage of solution) in figure 3.7 which shows the relative contribution of the 512 highest order terms to the solution for the peak potential as a function of the number of terms in the solution. It is clear that terms of increasing order become less and less significant. As an example consider the following: when M=1024, the highest 512 terms (50% of the terms) contribute 40% of the solution magnitude. However, for M=2048, the highest order 512 terms (25% of the terms included) contribute only 10% to the solution magnitude.

Conclusion

We have developed two models of the spinal cord and verified that they have been properly implemented. Additionally we have conducted an error analysis that will enable us to determine the number of frequency space samples necessary to obtain a solution with sufficient resolution for our purposes.

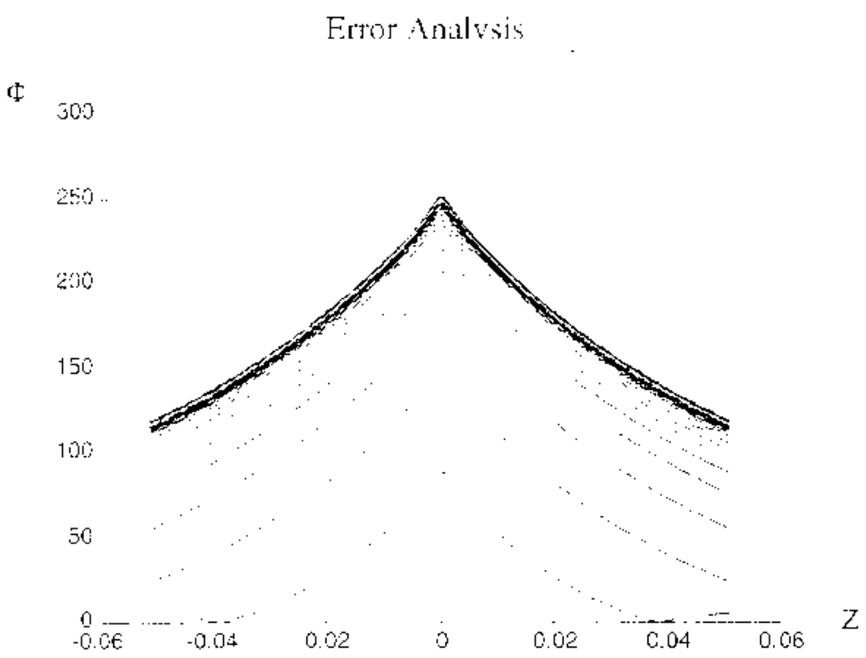

Figure 3.6. Potential as a function of position alonf the z-axis. Each curve is a solution with an additional 512 samples added in the z-frequency space (starting at the bottom). It is clear that as the terms are of increasingly higher order, they contribute less to the solution.

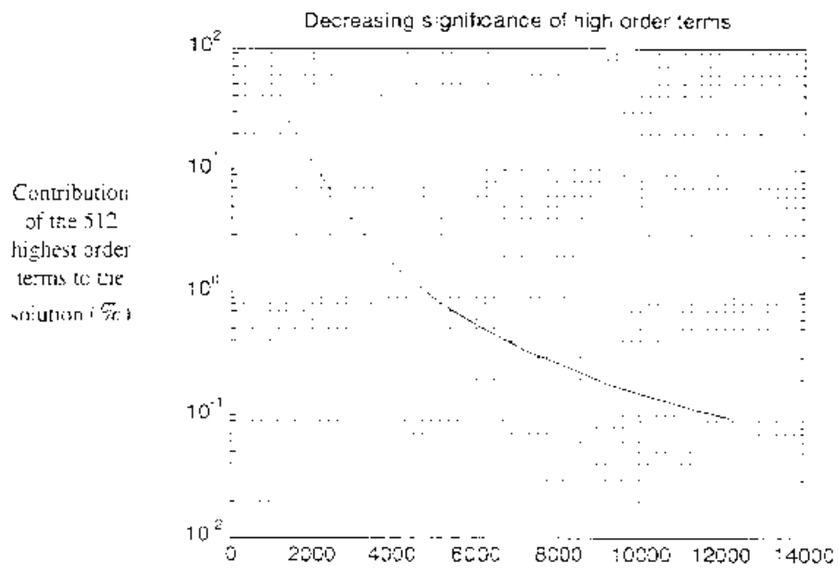

Figure 3.7: Contribution of the 512 highest order terms to the solution (as a %) as a function of the number of terms in the solution.

PUBLICATIONS THIS QUARTER

Barbeau, H., D.A. McCrea, M.J. O'Donovan, S. Rossignol, W.M. Grill, M.A. Lemay (1999) Tapping into spinal circuits to restore motor function. Brain Research Reviews 30:27-51.

Grill, W.M. B.O. Erokwu, S. Hadziefendic, M.A. Haxhiu (1999) Extended survival time following pseudorabies virus injection labels the suprapontine neural network controlling the bladder and urethra in the rat. Neuroscience Letters 270:63-66.

OBJECTIVES FOR THE NEXT QUARTER

In the next quarter we will continue our co-localization studies to identify inhibitory spinal neurons active during micturition. Our specific objective is to establish immunocytochemical methods to co-localize c-Fos with glycine, the primary inhibitory

neurotransmitter in the spinal cord. We will also continue our studies characterizing the hindlimb motor responses to lumbar microstimulation. Our specific objective is to investigate the hindlimb motor responses evoked in the decerebrate preparation by stimulating in the contralateral spinal cord. Finally, we will continue development of our electrical mapping method. Our specific objective is to implement the electrical field solution for a pair of concentric cylinders, where the outer cylinder has anisotropic conductivity (i.e., different conductivities in the radial and longitudinal directions), as has been documented for the spinal white matter.

LITERATURE CITED

Altman, K.W., R. Plonsey (1988) Development of a model for point source electrical fiber bundle stimulation. Med. Biol. Eng. Comput. 26:466-475.

Cornelis, J.P.H., E.H.G. Nyssen (1985) Potentials produced by arbitrary current sources in an infinite and finite-length circular conducting cylinder. IEEE Trans. Biomed. Eng. 32:993-1000

Giszter, S.F., F.A. Mussa-Ivaldi, E. Bizzi (1993) Convergent force fields organized in the frog's spinal cord. J. Neuroscience 13:467-491.

Grill, W.M., B. Wang, S. Hadziefendic, M.A. Haxhiu (1998a) Identification of the spinal neural network involved in coordination of micturition in the male cat. Brain Research 796:150-160.

Hoy, MG and RF Zernicke, "Modulation of limb dynamics in the swing phase of locomotion." J Biomech. 18(1 1985): 49-60.

Meier, J.H., W.L.C. Rutten, H.B.K. Boom (1998) Extracellular potentials from active myelinated fibers inside insulated and noninsulated peripheral nerve. IEEE Trans. Biomed. Eng. 45:1146-1153

Oostendorp, T.F., A. Van Oosterom (1989) Source parameter estimation in inhomogeneous volume conductors of arbitrary shape. IEEE Trans. Biomed. Eng. 36:382-391.